ARCHIVES OF ELECTRICAL ENGINEERING VOL. 67(4), pp. 755–772 (2018)

DOI 10.24425/aee.2018.124738

Modeling of an isolated induction generator considering saturation effect

EZZEDDINE TOUTI[1,2], HABIB KRAIM[1], REMUS PUSCA[3], RAPHAEL ROMARY[3]

[1] *College of Engineering, Northern Border University*
Arar, 1321, Saudi Arabia

[2] *ENSIT, University of Tunis*
5-Taha Hussein, Tunis-1008, Tunisia

[3] *Faculty of Applied Sciences, University of Artois*
Béthune, France
e-mail: touti.these09@gmail.com

(Received: 04.03.2018, revised: 18.07.2018)

Abstract: This paper proposes a self-excited induction generator model with saturation effect for power generating mode in a remote site. The model is led through the space vector mathematical formalism and allows one to analyze the steady and dynamic states. It is developed for a squirrel cage induction machine. This model provides magnetizing inductance variation able to influence the build-up and the stabilization of voltage generation when the load changes. The final result is a realistic approach model which takes into consideration the dependency of the magnetizing inductance versus magnetizing current. This novel model is validated through experimental measurements to demonstrate its validity and practicability.

Key words: induction generator, modeling, saturation effect, frequency analysis

1. Introduction

The wind energy seems to be a good promising alternative source which can accompany the classical energy sources [1–4]. The use of wind turbines is an attractive solution because they can provide energy at a competitive price and mainly it does not cause environmental contamination [5–8]. In isolated sites, the wind turbine equipped with a squirrel cage induction machine (IM) presents major benefits when extreme climatic conditions occur or when the demand for electric power is limited. This topic has received considerable attention in recent years in view of the suitability of induction generators. So, this wind generator is widely used because of its robustness, high reliability and low cost and maintenance [9–14].

Nevertheless, there are some difficulties in the use of this machine especially when it operates in autonomous mode as, for example, self-excitation procedure, frequency control and voltage control [15]. Indeed, these induction generators need an external supply providing the reactive power which is necessary for production of the rotating magnetic flux [16, 17].

The use of the self-excited induction generator (SEIG) has been revealed for a few decades and was implemented in some remote sites. A three-phase induction machine can operate as a self-excited generator when its rotor is driven by an external prime mover and its excitation is provided by connecting a three-phase capacitor bank at the stator terminals. In this condition, induced electromagnetic forces and currents in the stator windings start to rise and will continue until equilibrium is reached due to the magnetic saturation in the machine [18].

The aim of this paper is to present a new induction machine model which takes into account the magnetic saturation effect for analysis of the machine permanent and transient behavior. If the IM is simulated as a motor, the magnetizing inductance can be determined only for rated voltage but for self-excited induction generator simulation, a performing model requires values of the magnetizing inductance for whole voltage region. A proposed method for integration of inductance variation in the SEIG model is proposed in [19]. This method considers three possible cases of steady state values to estimate the nonlinearity of the magnetization curve and proposes sufficient large initial voltage to the capacitors to bring a high magnetizing current which allows fixing the generator in the stable mode.

Another method for estimation of magnetizing inductance variation is presented in [20] which proposes a variation curve as the function of the magnetizing current at the ideal no-load condition. However, in load condition the generator slip is not zero and the magnetizing inductance value changes.

The novel SEIG model presented in this paper is based on space phasor formalism. This model proposes the integration of an adaptive method for magnetizing curve identification with variation curve and practical calibration in load condition.

The first part of this paper deals with the SEIG modeling based on the space phasor formalism. The first section presents a linear model (the saturation effect is neglected) and the second section presents the new developed model of the SEIG considering the magnetic saturation phenomenon. The third section presents the magnetic inductance approximation proposed for the SEIG developed model. The fourth section concerns the simulation and experimental results considering an $R-L$ load. The influence of the saturation on the frequency control is discussed in the last part of this paper.

2. System configuration

Fig. 1 presents the considered system configuration for a self-excited induction generator which operates in a remote site. Driven by the wind, this induction generator will provide electrical power to supply a variable inductive-resistive load placed in parallel. A capacitor bank of capacitance C provides the reactive power required for machine magnetization and assures the reactive power required by the load.

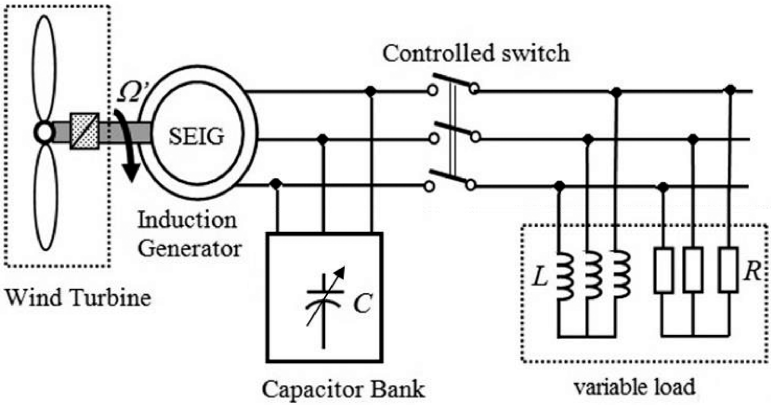

Fig. 1. Schematic diagram of a SEIG in autonomous mode

3. Self-excited induction generator model

The real machines, with their different kinds of windings and geometries, are too complex for analysis taking into account their real configurations, hence it is needed to develop a model, the behavior of which is as close as possible to that of the original one [21].

In this context, it is essential to use a simple model to facilitate numerical implementation and to minimize the simulation computation time. To study the transient and steady state of the asynchronous generator, the SEIG model using space phasor formalism is implemented in the Matlab Simulink environment. Let us consider a p pole pair rotor cage induction machine with a three-phase equivalent rotor winding. The rotor and stator spatial reference (d^r and d^s) are tied to the rotor and stator phase 1 axes. To produce the stator voltage, the induction generator must have a rotor residual magnetic field [22, 23]. A fictitious winding is considered in the model to create this magnetic field during the SEIG start-up step. The variables corresponding to these fictitious windings are labeled with the superscript "a". One considers that these windings of n^a turns are supplied by a $\bar{i}_q^a$ DC currents ($q = 1$, 2 or 3) and their sum is null after the start-up step. Let us denote $\bar{x}^s$ the stator space phasor variables defined relatively to d^s. The rotor space phasor variable defined relatively to d^r is written $\bar{x}^r$. $\bar{x}'^s$ is a stator space phasor variable defined relatively to the spatial reference d^r. Consequently one can deduce $\bar{x}'^s$ from $\bar{x}^s$ by means of the variable change $\bar{x}'^s = \bar{x}^s \exp(-j\theta)$, where $\theta = \omega' t + \theta_0$ represents the spatial angular gap between d^r relatively to d^s and $\omega' = p\Omega'$. Ω' is the rotor angular speed and p is the number of pole pairs of the induction machine.

3.1. Model without saturation effect

Let us consider that the studied induction machine is characterized by the parameters given in the appendix. This section shows the induction generator model developed without taking into account the magnetic saturation effect. In this case the voltage equations which characterize the

induction machine written in the rotor reference frame are given by the following system:

$$\begin{cases} \bar{v}'^s = r^s \bar{i}'^s + \dfrac{\mathrm{d}}{\mathrm{d}t}\bar{\varphi}'^s + j\omega'\bar{\varphi}'^s \\ \bar{v}^r = r^r \bar{i}^r + \dfrac{\mathrm{d}}{\mathrm{d}t}\bar{\varphi}^r \\ \bar{v}^a = r^a \bar{i}^a + \dfrac{\mathrm{d}}{\mathrm{d}t}\bar{\varphi}^a \end{cases}, \tag{1}$$

where r represents the per phase winding resistances. $\bar{\varphi}'^s$, $\bar{\varphi}^r$ and $\bar{\varphi}^a$ represent the fluxes linked by the stator (defined in the rotor reference frame), the rotor and the fictitious windings, respectively, expressed by:

$$\begin{cases} \bar{\varphi}'^s = (L^s + l^s)\bar{i}'^s + M^{sr}\bar{i}^r + M^{sa}\bar{i}^a \\ \bar{\varphi}^r = (L^r + l^r)\bar{i}^r + M^{rs}\bar{i}'^s + M^{ra}\bar{i}^a \\ \bar{\varphi}^a = (L^a + l^a)\bar{i}^a + M^{as}\bar{i}'^s + M^{ar}\bar{i}^r \end{cases}, \tag{2}$$

where l^s and l^r are, respectively, the rotor and stator leakage inductances, l^a is the leakage inductance of the considered fictitious windings. M^{sr}, M^{sa} and M^{ra} are the mutual inductances between the stator, the rotor and the fictitious windings. It will be considered that $M^{sr} = M^{rs}$, $M^{as} = M^{sa}$ and $M^{ra} = M^{ar}$. The L quantities appearing in (2) are the main winding cyclic inductances and M is the mutual inductance between the different windings. It is assumed that the induction machine turn ratio at standstill is close to $n^s/n^r = \sqrt{2}$, with $L^r = L^s/2$. Let us consider the main cyclic winding inductance of the fictitious windings of the tested machine $L^a = (M^{sa})^2/L^s$. This value of L^a has been chosen in such a way that the fictitious winding can provide the starting current for the SEIG. In this case the M inductance can be expressed as:

$$\begin{cases} M^{sr} = \sqrt{L^s L^r} = L^s/\sqrt{2} \\ M^{sa} = \sqrt{L^s L^a} \\ M^{ra} = \sqrt{L^r L^a} \end{cases}. \tag{3}$$

For this model where the magnetic saturation effect is neglected, all the main and the mutual inductance coefficients are constant. Using Equations (1) and (2), the stator voltage defined in the d^r reference frame is given by:

$$\bar{v}'^s = \left[r^s + j\omega'(L^s + l^s)\right]\bar{i}'^s + (L^s + l^s)\frac{\mathrm{d}\bar{i}'^s}{\mathrm{d}t} + j\omega' M^{sr}\bar{i}^r + M^{sr}\frac{\mathrm{d}\bar{i}^r}{\mathrm{d}t} + j\omega' M^{sa}\bar{i}^a. \tag{4}$$

Considering the R–L load, the SEIG output current can be written as:

$$\bar{i}'^s = -\left(\frac{\bar{v}'^s}{R} + C\frac{\mathrm{d}\,\bar{v}'^s}{\mathrm{d}t} + \frac{1}{L}\int \bar{v}'^s\,\mathrm{d}t\right). \tag{5}$$

The stator angular frequency $\omega$is calculated taking into account the slip s obtained from: $\Omega' = (1 - s)\Omega$ and the synchronous angular speed $\Omega = \omega/p$. Moreover, to model this SEIG during transients and steady states, a mechanical relationship has to be considered:

$$T_w = T_e + T_f + J\frac{\mathrm{d}\,\Omega'}{\mathrm{d}t}, \tag{6}$$

where J is the overall system inertia, T_f is the SEIG friction and windage torque and T_w the torque which acts on the SEIG shaft by mean of the blades. The T_e machine electromagnetic torque is defined by the following cross product:

$$T_e = 3p\left(\bar{\varphi}'^s \times \bar{i}'^s\right)/2. \tag{7}$$

3.2. Model considering saturation effect

Generally, the induction machine model includes constant parameters. This model can be convenient to describe the fundamental air-gap flux density characteristics in a limited range of operating condition. However, when the operating point varies, as is the case in isolated induction generator, some parameters of the machine may change due to variations of the flux magnitude, voltage and the frequency. For these reasons, it is advisable to investigate an induction generator model which takes into account the magnetic saturation. In many works, the magnetizing inductance is considered constant or having a model which does not reflect the real phenomenon during start-up step of the induction generator and its self-excitation. The inductances vary slightly and can be considered constant at low flux values. But when the flux increases the machine starts to saturate and the inductances vary greatly. The induction machine is usually designed to be slightly saturated at the rated operating point to maximize the torque production [24].

If the machine is used as a wind generator, the operating point and the system evolution to the steady state depend on the magnetic circuit saturation. The performances of induction machines which operate in saturation condition have been investigated in several papers and some adapted models are suggested [25–28]. The most accurate method is to define the exact geometry of the studied machine. Then the Maxwell equations associated with the laws of used materials behavior are solved by the mean of numerical methods (finite element). Nevertheless, this method remains difficult to apply because it requires a large computing time. In the presented work the saturation will be taken into account by considering an approximation of the magnetizing inductance as a function of the magnetization current. This work is achieved considering that all the leakage inductances are constant. This hypothesis is largely verified since the leakage flux paths are in the air. In the following developments, it will be assumed that $L^s = L_m$ which represents the magnetizing inductance. The magnetizing current i_m is expressed as:

$$\bar{i}_m = \bar{i}'^s + \bar{i}^r\,. \tag{8}$$

By deriving the equations of the fluxes linked by the stator, the rotor and the fictitious windings given by (2), one obtains the time derivative of the magnetizing inductance L_m. Consequently, the expressions given by (2) can be written as follows:

$$\begin{cases} \dfrac{\mathrm{d}\,\bar{\varphi}'^s}{\mathrm{d}\,t} = \dfrac{\mathrm{d}\,L_m}{\mathrm{d}\,i_m}(\bar{i}'^s + \gamma\bar{i}^r + \chi\bar{i}^a)\cdot\left(\dfrac{\mathrm{d}\,\bar{i}'^s}{\mathrm{d}\,t} + \dfrac{\mathrm{d}\,\bar{i}^r}{\mathrm{d}\,t}\right) + (L_m + l^s)\dfrac{\mathrm{d}\,\bar{i}'^s}{\mathrm{d}\,t} + \gamma L_m\dfrac{\mathrm{d}\,\bar{i}^r}{\mathrm{d}\,t} \\ \dfrac{\mathrm{d}\,\bar{\varphi}^r}{\mathrm{d}\,t} = \dfrac{\mathrm{d}\,L_m}{\mathrm{d}\,i_m}(\gamma\bar{i}'^s + \delta\bar{i}^r + \eta\bar{i}^a)\cdot\left(\dfrac{\mathrm{d}\,\bar{i}'^s}{\mathrm{d}\,t} + \dfrac{\mathrm{d}\,\bar{i}^r}{\mathrm{d}\,t}\right) + (\delta L_m + l^r)\dfrac{\mathrm{d}\,\bar{i}^r}{\mathrm{d}\,t} + \gamma L \\ \dfrac{\mathrm{d}\,\bar{\varphi}^a}{\mathrm{d}\,t} = \dfrac{\mathrm{d}\,L_m}{\mathrm{d}\,i_m}(\chi\bar{i}'^s + \eta\bar{i}^r + \xi\bar{i}^a)\cdot\left(\dfrac{\mathrm{d}\,\bar{i}'^s}{\mathrm{d}\,t} + \dfrac{\mathrm{d}\,\bar{i}^r}{\mathrm{d}\,t}\right) + \chi L_m\dfrac{\mathrm{d}\,\bar{i}'^s}{\mathrm{d}\,t} + \eta L_m\dfrac{\mathrm{d}\,\bar{i}^r}{\mathrm{d}\,t} \end{cases}, \tag{9}$$

Taking into account the relationship (3), the different parameters of (9) are:

$$\gamma = 1/\sqrt{2}, \qquad \delta = 1/2, \qquad \eta = \sqrt{L^a/2L^s}, \qquad \xi = L^a/L^s \quad \text{and} \quad \chi = \sqrt{L^a/L^s}.$$

In this case, the equations given by (1) can be expressed as:

$$\begin{cases} \bar{v}'^s = \left(\alpha\dfrac{\mathrm{d}\,L_m}{\mathrm{d}\,i_m}+\gamma L_m\right)\cdot\left(\dfrac{-r^r}{K_{2r}}\bar{i}^r\right)+\left[\alpha\dfrac{\mathrm{d}\,L_m}{\mathrm{d}\,i_m}+L_m+l^s-\dfrac{K_{1r}}{K_{2r}}\bar{i}^r\left(\alpha\dfrac{\mathrm{d}\,L_m}{\mathrm{d}\,i_m}+\gamma L_m\right)\right]\dfrac{\mathrm{d}\,\bar{i}'^s}{\mathrm{d}\,t}+ \\ \qquad +j\omega'\left[(L_m+l^s)\bar{i}'^s+\gamma L_m\bar{i}^r+\chi L_m\bar{i}^a\right]+r^s\bar{i}'^s \\ 0 = r^r\bar{i}^r+\left(\beta\dfrac{\mathrm{d}\,L_m}{\mathrm{d}\,i_m}+\gamma L_m\right)\dfrac{\mathrm{d}\,\bar{i}'^s}{\mathrm{d}\,t}+\left(\beta\dfrac{\mathrm{d}\,L_m}{\mathrm{d}\,i_m}+\delta L_m+l^r\right)\dfrac{\mathrm{d}\,\bar{i}^r}{\mathrm{d}\,t} \end{cases}, \tag{10}$$

where

$$\begin{cases} \alpha = \bar{i}'^s+\gamma\bar{i}^r+\chi\bar{i}^a, & \beta = \gamma\bar{i}'^s+\delta\bar{i}^r+\eta\bar{i}^a, \\ K_{1r} = \beta\dfrac{\mathrm{d}\,L_m}{\mathrm{d}\,i_m}+\gamma L_m, & K_{2r} = \beta\dfrac{\mathrm{d}\,L_m}{\mathrm{d}\,i_m}+\delta L_m+l^r. \end{cases} \tag{11}$$

From (10) we can deduce the following relationship:

$$\begin{aligned} \frac{\mathrm{d}\,\bar{i}'^s}{\mathrm{d}\,t} = & \frac{\bar{v}'^s-\left(\alpha\dfrac{\mathrm{d}\,L_m}{\mathrm{d}\,i_m}+\gamma L_m\right)\cdot\left(\dfrac{-r^r}{K_{2r}}\bar{i}^r\right)}{\left[\alpha\dfrac{\mathrm{d}\,L_m}{\mathrm{d}\,i_m}+L_m+l^s-\dfrac{K_{1r}}{K_{2r}}\bar{i}^r\left(\alpha\dfrac{\mathrm{d}\,L_m}{\mathrm{d}\,i_m}+\gamma L_m\right)\right]} \\ & +\frac{-j\omega'\left[(L_m+l^s)\bar{i}'^s+\gamma L_m\bar{i}^r+\chi L_m\bar{i}^a\right]-r^s\bar{i}'^s}{\left[\alpha\dfrac{\mathrm{d}\,L_m}{\mathrm{d}\,i_m}+L_m+l^s-\dfrac{K_{1r}}{K_{2r}}\bar{i}^r\left(\alpha\dfrac{\mathrm{d}\,L_m}{\mathrm{d}\,i_m}+\gamma L_m\right)\right]}. \end{aligned} \tag{12}$$

The numerical implementation in the Matlab/Simulink environment of Equation (12) is shown in Fig. 2. The Ts, which appears in Fig. 2 is the sample time used in numerical model and less or equal to 5.10^{-5} for this application.

The detailed diagram of Fig. 2 is developed in the appendix. Fig. 3 shows the numerical implementation of the equations giving K_{1r} and K_{2r}.

The electromagnetic torque can be defined as a function of magnetizing inductance by Expression (13) and its implementation is shown by Fig. 4:

$$T_e = \frac{3}{2}p\left[(L_m+l^s)\bar{i}'^s+\gamma L_m\bar{i}^r+\chi L_m\bar{i}^a\right]\times\bar{i}'^s. \tag{13}$$

Finally, the numerical implementation of the mechanical equation given by Expression (6) will be presented by Fig. 5.

The numerical implementation of the already presented blocs allows the simulation of the stator voltage variations (amplitude and frequency) during transient and steady state considering the numerical values given in the appendix.

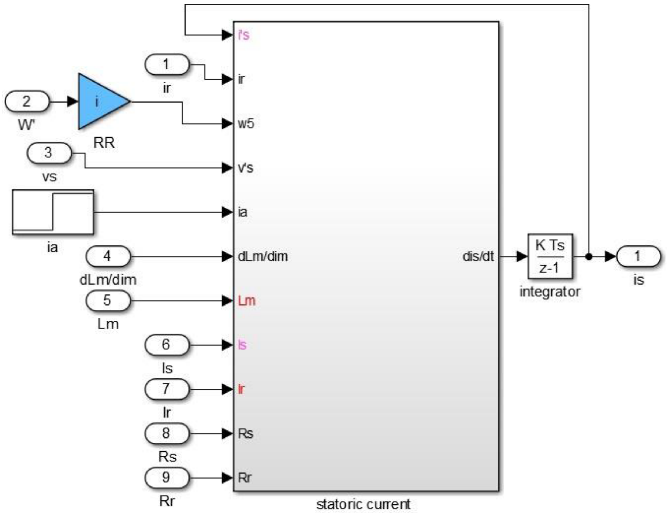

Fig. 2. Statoric current implementation

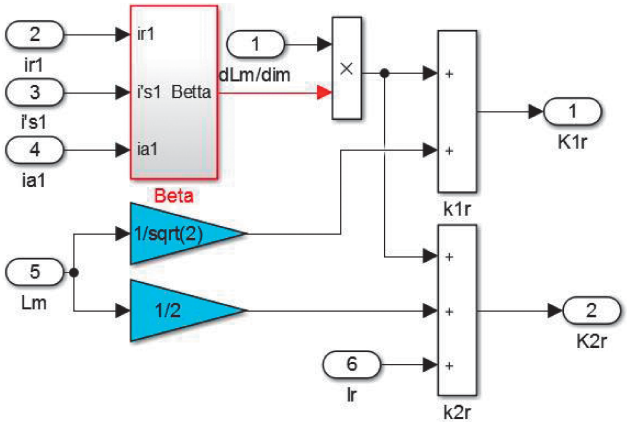

Fig. 3. Implementation of K_{1r} and K_{2r}

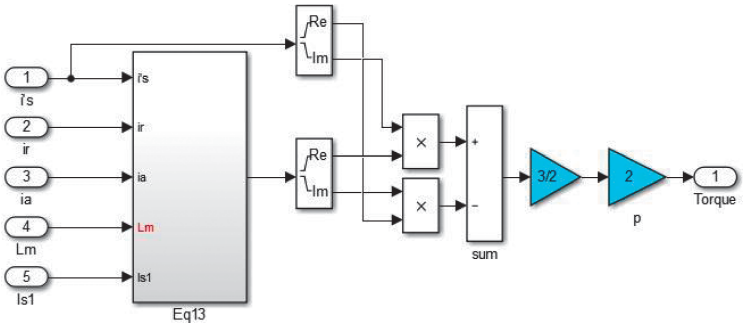

Fig. 4. Electromagnetic torque implementation

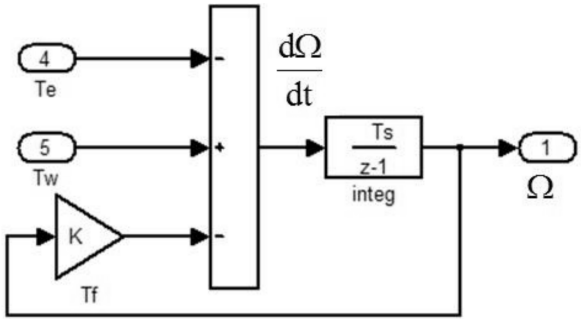

Fig. 5. Mechanical equation implementation

4. Magnetizing inductance approximation

Considering an IM in the motor operation case, it is possible to determine its magnetizing inductance at the rated voltage and so to model the induction machine. Nevertheless, in the case of an isolated generator when neither the frequency nor the voltage is imposed it is essential to have the values of the magnetizing inductance with accuracy for the whole voltage range of the used machine.

For magnetizing inductance estimation, the machine operates as an induction motor. Under no-load conditions, the procedure starts by increasing the stator voltage slowly up from zero while the rotor speed is kept at synchronous speed by an external prime mover that provides the mechanical losses of the IM. The magnetizing current and the voltage are measured at the terminals of the machine. The evolution of the magnetizing inductance versus magnetizing current is given by Fig. 6. This curve is obtained by testing the machine with parameters determined at the rated frequency (50 Hz).

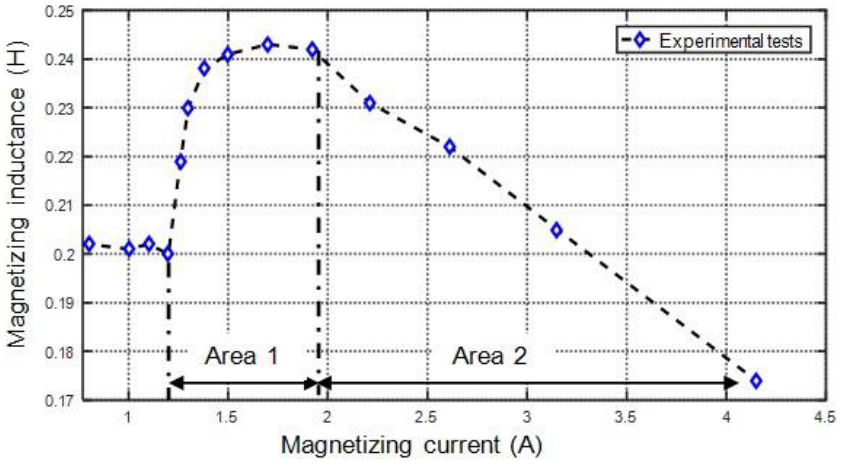

Fig. 6. Magnetizing inductance versus magnetizing current

The determination of the magnetizing inductance as a function of the magnetizing current $L_m = f\,(i_m)$ can be carried out using different approaches. In this study, it is proposed to consider different areas depending on the magnetizing current L_m is defined as:

$$L_m = \begin{cases} 0.2\ \text{H} & \text{for } i_m \leq 1.2\ \text{A} \\ ai_m^4 + bi_m^3 + ci_m^2 + di_m - h & \text{for } 1.2\ \text{A} < i_m \leq 1.92\ \text{A} \quad \text{(Area 1)}, \\ qe^{-\tau i_m} & \text{for } i_m > 1.92\ \text{A} \quad \text{(Area 2)} \end{cases} \tag{14}$$

where a, b, c, d and h are the numerical parameters obtained by identification of the fourth order equation in (14) considering the measured values of the magnetizing inductance. These values lead to a similar curve as that presented in Fig. 6. They are: $a = 1.3247$, $b = 8.6762$, $c = 21.247$, $d = 23.07$, $h = 9.1338$, $q = 0.3207$ and $\tau = 0.145$.

According to the results given in Fig. 6, the values of L_m increase to reach the maximum in Area 1, which corresponds to the machine start-up time, characterized by important voltage variation, and which is considered as an unstable area. Here, any decrease in the speed causes a decrease in the voltage and consequently the disengagement of the generator leading to a total demagnetization of the machine. This demagnetization can cause difficulties in the self-excitation step. If it appears, a specific procedure must be applied to recover the residual magnetic field and to restart the generator. However in Area 2, the magnetizing inductance values decreases if the voltage increases enabling the generator to continue to operate. This region is considered as a stable-operating region where the SEIG must operate.

5. Simulation and experimental results

5.1. Experimental test bench

To validate the simulation results obtained by the developed model that takes into account the magnetic saturation effects, the experimental test bench of Fig. 7 uses a three-phase, delta-connected cage induction machine. The generator is connected to a three-phase resistive-inductive

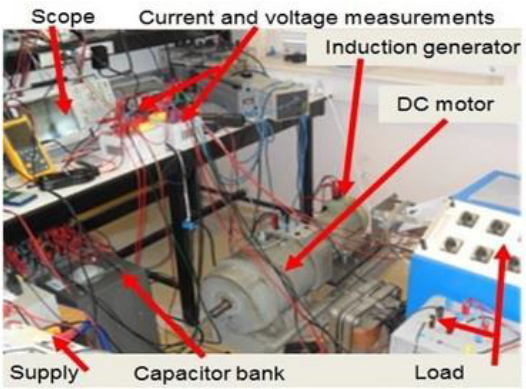

Fig. 7. Experimental test bench of the SEIG

load and a three-phase capacitor bank that allows providing the reactive power required by the induction machine and the load. Their values are chosen such that the generator operates at rated voltage in the steady state. It is driven by a DC motor which operates at constant magnetic flux, mechanically connected to the IM which operates as a SEIG. For a target $R-L$ load, the study starts by finding, by means of numerical simulation, the adequate pair (R, C) which, physically, consists in keeping constant the argument of the elements connected to the SEIG outputs.

The experiment has been done at variable wind power P_w which acts on the blades with a target load characterized by R_0, C_0 and keeping the load $L = 0.170$ H at constant value. The characteristics of the three-phase induction machine used for simulation and experiments as a SEIG are given in the appendix.

5.2. Modeling of the SEIG magnetizing inductance curve

In Fig. 8, the first part of the curve (Area 1) has been determined from the no load motor tests. The second part (Area 2) can be determined after loading the generator. The second part of the curve is obtained by the experimental SEIG steady-state considering four different loads.

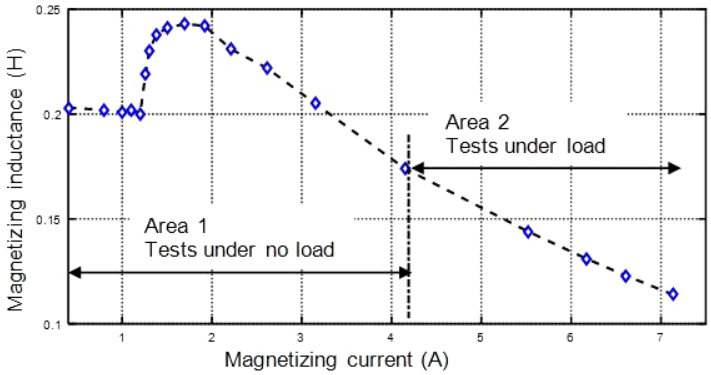

Fig. 8. Extended magnetizing inductance curve proposed for the SEIG

To validate the magnetizing inductance variation used in numerical model, the values obtained by approximation of the curve are compared with measured ones.

5.3. Experimental study with load switching

In order to validate the developed model which takes in consideration the magnetizing inductance variation, different loads used in the simulation model were tested experimentally. The implementation of the variable magnetizing inductance in the proposed SEIG model is important for any induction generator which must operate in the saturated state. In order to validate the new developed model which takes into account the magnetizing inductance variation, four loads used in simulation model were also tested in the experimental test bench.

Table 1 summarizes the tests carried out for an $R-L$ load ($R_0 = 35\ \Omega$, $C_0 = 145\ \mu$F) with a constant load $L = 0.170$ H. The calibration of the simulation model allows us to obtain the inductance variation as voltage or a current function.

Table 1. First experimental test for calibration of the SEIG model (R_0 = 35 Ω, C_0 = 145 μF) with L_m variable

Experimental values			**Simulation values**			
U (V)	**I (A)**	**F (Hz)**	**U (V)**	**I (A)**	**F (Hz)**	**L_m (H)**
415.8	10.7	56.5	415.7	10.8	56.3	0.114
381	9.45	54.9	381	9.5	54.9	0.123
347.3	8.35	53.6	347.1	8.5	53.7	0.131
286.7	7.2	52.3	287	6.84	52.4	0.144

The results presented in Table 1, shows that the increase of the voltage leads to a decrease of the magnetizing inductance and consequently the frequency increases. So, an approximation curve must be introduced in the SEIG modeling with the L_m variable to consider the magnetic saturation effect. Fig. 9 presents the evolution of the proposed approximation curve using the relationship (14).

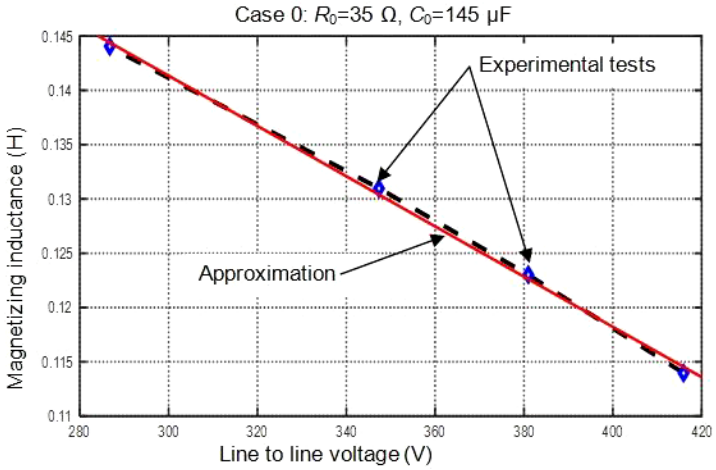

Fig. 9. Magnetizing inductance curve and approximated one

To validate the simulation model, firstly, the experimental values presented in Table 1 are used for calibration of the SEIG parameters used in the simulation model. In the second test, another higher load (R_1 = 28 Ω and C_1 = 62.5 μF) is used in order to confirm the localization of L_m in the range already estimated by (14) and presented in Area 2 of Fig. 8. The obtained experimental and simulation results are shown in Table 2. It can be remarked that the values are close.

The magnetizing inductance variation for the second load compared to the first one is presented in Fig. 10, where the identical variation is shown. It allows a comparative study of the variation of the magnetizing inductance between the two states of the load.

The case, where the inductance variation is not considered in the simulation model is presented in Table 3. For this case, a significant difference, obtained between the experimental results and

Table 2. Second experimental test for validation of SEIG model (R_1 = 28 Ω, C_1 = 162.5 μF) with L_m variable

Experimental results			Simulation results			
U (V)	**I (A)**	**F (Hz)**	**U (V)**	**I (A)**	**F (Hz)**	**L_m (H)**
378	11.6	54.8	377.6	11.5	54.23	0.1235
358	10.9	54.2	358.1	10.7	53.85	0.128
334	10	53.5	334.3	9.85	53	0.1335

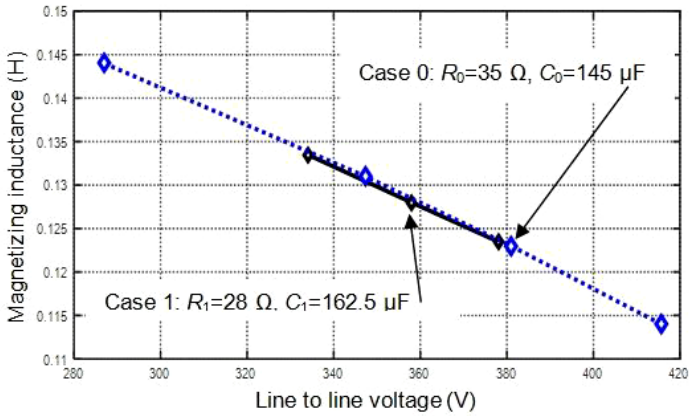

Fig. 10. Magnetizing inductance versus line-to-line voltage for loads R_0C_0 and R_1C_1

simulation ones concerning the current and the frequency, is noticed. So, it can be concluded that the proposed extended curve method is satisfactory for integration in the new **SEIG** model.

Table 3. First studied case used for calibration of the SEIG model with L_m constant R_0 = 35 Ω, C_0 = 145 μF

Experimental values			Simulation values			
U (V)	**I (A)**	**F (Hz)**	**U (V)**	**I (A)**	**F (Hz)**	**L_m (H)**
415.8	10.7	56.5	415.7	10.7	56.3	0.114
381	9.45	54.9	381	9.87	56.28	0.114
347.3	8.35	53.6	347.1	8.99	56.29	0.114
286.7	7.2	52.3	287	7.42	56.28	0.114

5.4. Frequency estimation for load variation

This novel **SEIG** model has been developed to obtain more precision in frequency and voltage estimation for an isolated induction generator feeding a L load and a variable resistive

load. So in following tests, the L load is considered constant and only L_m can vary. Therefore, one performs variation of the R–C load from $R_0 = 35\ \Omega$ and $C_0 = 145\ \mu$F to $R_1 = 28\ \Omega$, and $C_1 = 162.5\ \mu$F. This switching load, starting at time 5 s, is carried out keeping the voltage at quasi constant value. Consequently the magnetizing inductance L_m is kept constant in the first simulation test (Fig. 11(a) – dashed line) and variable in the second test (Fig. 11(a) – solid line). The switching load at variable voltage is shown in Fig. 11(b). Two cases are presented, the first one is presented by the dashed line curve, which reveals the switching in constant magnetizing inductance ($L_m = 0.123$ H). The second case is presented by the curves plotted with a solid line. It reveals the case when L_m varies ($L_m = 0.128$ H) according to the results summarized in Table 4.

Table 4. Load variation from case 0 to case 1

	U (V)	**F (Hz)**	**I (A)**	***L_m* (H)**
Case 0: $R_0 = 35\ \Omega$, $C_0 = 145\ \mu$F	381	54.9	9.5	0.123
Case 1: $R_1 = 28\ \Omega$, $C_1 = 162.5\ \mu$F at L_m = constant	377.6	54.23	11.5	0.1235
Case 1: $R_1 = 28\ \Omega$, $C_1 = 162.5\ \mu$F at L_m = variable	358.1	53.85	10.7	0.128

The instantaneous values of the current at the outputs of the generator are represented by Figs. 11(c) and 11(d). This current is obtained by varying the voltage by mean of the load change. This voltage variation appears at $t = 5$ s. In Fig. 11(c), the switching from case 0 ($R_0 = 35\ \Omega$ and $C_0 = 145\ \mu$F) to case 1 ($R_1 = 28\ \Omega$ and $C_1 = 162.5\ \mu$F) leads to a difference between the rotor angular speed obtained with the SEIG model which considers Lm constant and the model which considers L_m as a variable parameter.

Consequently, the current frequency is different as can be seen in Fig. 11(d). This frequency gap between the two simulation models is due to the difference between two states of the magnetizing inductance and the choice of the model is dependent on the precision needed in the study of the SEIG implementation system.

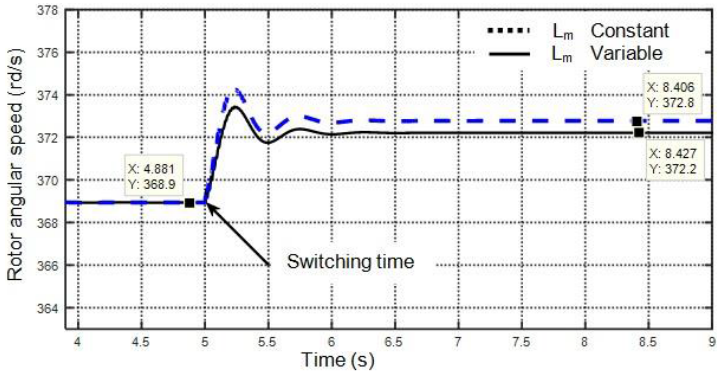

(a)

Fig. 11

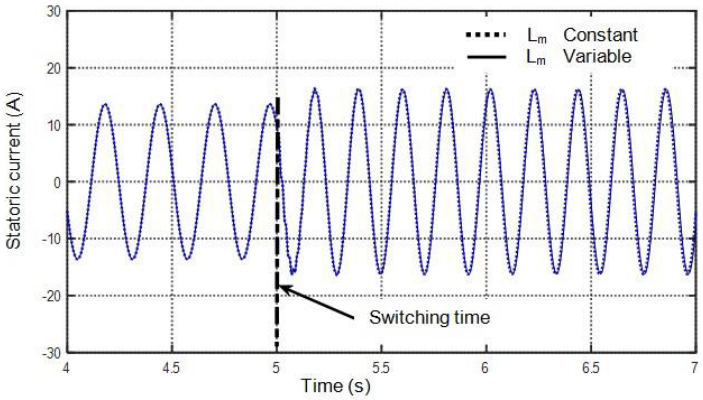

(b)

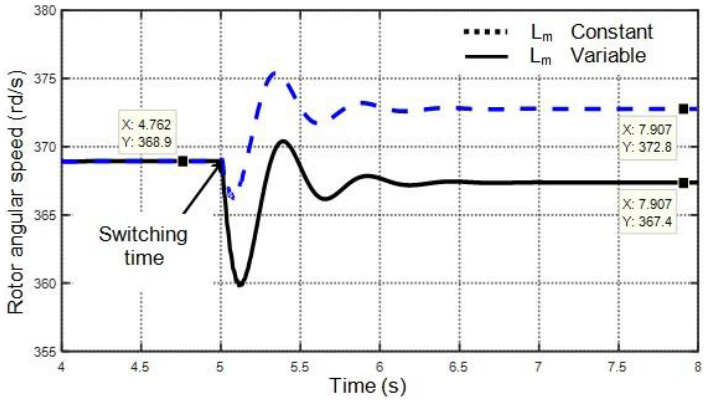

(c)

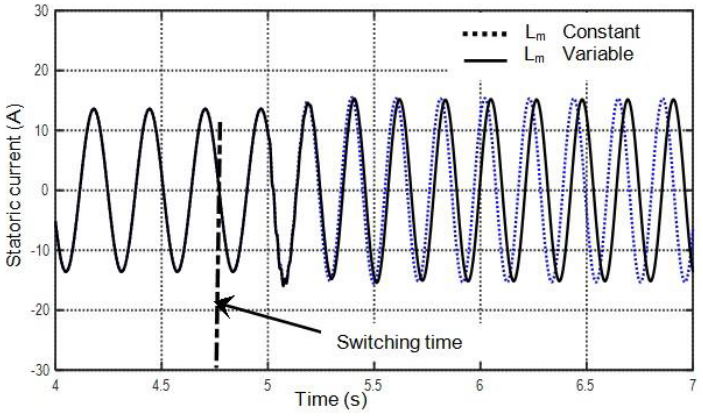

(d)

Fig. 11. Variation of the rotor angular speed and the stator current during load variation: (a) speed at constant voltage; (b) instantaneous current at constant voltage; (c) speed at variable voltage; (d) instantaneous current at variable voltage

6. Saturation influence in frequency stabilization

The frequency control strategy consists in maintaining at a constant value the argument of the whole load and capacitor, which are connected in parallel to the SEIG terminal. In this case, it is possible to obtain an operation at quasi-constant frequency without introducing any control loop of this variable. This state is achieved when a suitable choice of the load is realized in accordance with the generator parameters and the voltage target is realized. Let us consider that φ is the argument of the elements connected to the SEIG terminal, in the case of an inductive-resistive load, keeping $\tan\varphi = \text{const}$ leads to maintain constant the following relationship [29]:

$$R[LC\omega^2 - 1] = \text{const}. \tag{15}$$

Starting with the operating point obtained for R_0 and C_0, the changes of R must be accompanied by changes of the C capacitor in order to maintain the frequency ω at practical value close to the initial one. That needs to satisfy the following equality:

$$R_0[LC_0\omega^2 - 1] = R_1[LC_1\omega^2 - 1]. \tag{16}$$

Nevertheless, starting from the load $R_0 = 35\ \Omega$ and $C_0 = 145\ \mu$F, the switching to $R_1 = 28\ \Omega$ and $C_1 = 162.5\ \mu$F was carried out without applying the law given by the relationship (16) because the saturation affects the inductances of the machine. Thereby the reactive power demanded by the generator varies. Consequently, the capacitor changes accordingly to this variation, which leads to a shift in the frequency values as it is shown in the results given by Table 1 and Fig. 11.

According to the simulation and experimental results, we can remark that the load variation and the saturation have an influence on the SEIG frequency. For this reason, the model of the SEIG developed in this work which takes into consideration the inductance variation as the function of magnetizing current is more convenient to obtain more accurate simulation results. Furthermore if the SEIG working temperature is high, the permeability and inductance variation must be considered and the model improved, including the second law for harmonizing the inductance variation with the temperature [30].

7. Conclusion

This paper analyses the influence of the magnetic saturation effect in the self-excited induction generator working in an isolated grid. This work proposes a novel analytical model able to take in consideration this effect when the induction generator operates at variable load in the saturation area. In order to take into account the magnetizing inductance variation, a simple approximation law which gives accurate results is proposed in this paper. The presented law considers two working areas of the SEIG and proposes the classical identification procedure of the magnetizing inductance characteristic. This method is based on the standards motor tests for the analytical model. This model can be used to predetermine with good accuracy the required capacitance, voltage and frequency values in concordance with the considered load. However, for good results in the wind power variation, the simulation model needs, in the first time, a calibration step with a few operating points of the machine working as a generator.

Appendix

The characteristics of the used three-phase induction machine are given by: 380 V/660 V, 7.3 A/4.2 A, 7.5 kW, 1420 rpm, p = 2, F = 50 Hz, $\cos\Phi$ = 0.8, r^r = 3 Ω, r^s = 8.66 Ω, r^a = 10 Ω, M^{ra} = 70.6 mH, M^{sa} = 100 mH, M^{sr} = 377 mH, L^s = 534 mH, J = 0.05 Kg·m^2, L^a = 18.7 mH, l^a = 5 mH, L^r = 26 mH, l^r = 4 mH, l^s = 27 mH.

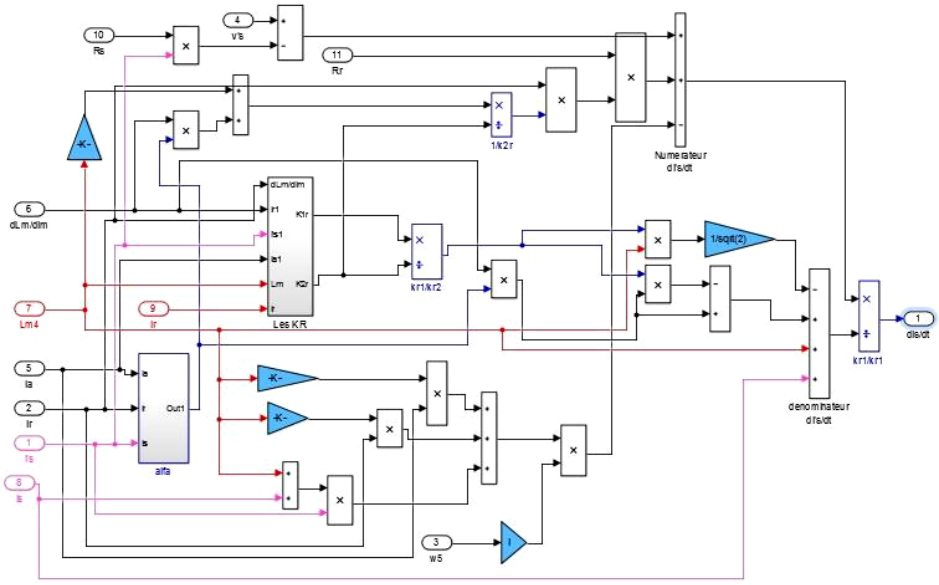

Fig. 12. detailed diagram of Fig. 2

Acknowledgements

The authors gratefully acknowledge the approval and the support of this research study by the grant No. 4675-ENG-2016-1-6-F from the Deanship of Scientific Research at Northern Border University, Arar, KSA.

References

[1] Herbert G.M.J., Iniyan S., Sreevalsan E., Rajapandian S., *A review of wind energy technologies*, Renewable and Sustainable Energy Reviews, vol. 11, no. 6, pp. 1117–1145 (2007).

[2] Rahim A.H.M.A., Ahsanul Alam M., Kandlawala M.F., *Dynamic performance improvement of an isolated wind turbine induction generator*, Computers and Electrical Engineering, vol. 35, no. 4, pp. 594–607 (2009).

[3] Tudorache T., Bostan V., *Wind Generators Test Bench. Optimal Design of PI Controller*, Advances in Electrical and Computer Engineering, vol. 11, no. 3, pp. 65–70 (2011).

[4] Mihet-Popa L., Groza V., *Modeling and Simulation of a 12 MW Wind Farm*, Advances in Electrical and Computer Engineering, vol. 10, no. 2, pp. 141–144 (2010).

[5] Gaurav K.K., Bhim S., *Voltage and frequency controllers for an asynchronous generator-based isolated wind energy conversion system, IEEE Transaction on Energy Conversion*, vol. 26, no. 2, pp. 402–416 (2011).

[6] Deng Y.Y., Kornelis B., van der Leun K., *Transition to a fully sustainable global energy system*, Energy Strategy Reviews, vol. 1, iss. 2, pp. 109–121 (2012).

[7] Wang Y., Silva V., Lopez-Botet-Zulueta M., *Impact of high penetration of variable renewable generation on frequency dynamics in the continental Europe interconnected system*, IET Renewable Power Generation, vol. 10, no. 1, pp. 10–16 (2016).

[8] Ekanayake, J., *Induction generators for small hydro schemes*, IET Power Engineering, vol. 16, no. 2, pp. 61–67 (2002).

[9] Dawit, S., Colin G., Muhammed Fazlur R., *The dynamic characteristics of an isolated self-excited induction generator driven by a wind turbine*, IEEE Transaction on Industrial Application, vol. 39, no. 4, pp. 936–944 (2003).

[10] Chtchetinine O., *Voltage stabilisation system for induction generator in standalone mode*, IEEE Transaction on Energy Conversion, vol. 24, no. 2, pp. 936–944 (2009).

[11] Haque M.H., *A novel method of evaluating performance characteristics of a self-excited induction generator*, IEEE Transaction on Energy Conversion, vol. 14, no. 3, pp. 358–365 (1999).

[12] Bansal R.C., *Three-phase self-excited induction generators: An Overview*, IEEE Transaction on Energy Conversion, vol. 20, no. 2, pp. 292–299 (2005).

[13] Seyoum D., Grantham C., Rahaman F., *The dynamic characteristics of an isolated self-excited induction generator driven by a wind turbine*, IEEE Transaction on Industrial Application, vol. 39, no. 4, pp. 936–944 (2003).

[14] Lopes L.A.C., Almeida R.G., *Wind-driven self-excited induction generator with voltage and frequency regulated by a reduced rating voltage source inverter*, IEEE Transaction on Energy Conversion, vol. 21, no. 2, pp. 297–304 (2006).

[15] Alolah A.L., Alkanthal M.A., *Optimization based steady state analysis of three phase SEIG*, IEEE Transaction on Energy Conversion, vol. 15, no. 1, pp. 61–65 (2000).

[16] Ahmed T., Noro Hiraki O., Nakaoka E.M., *Terminal voltage regulation characteristics by static var compensator for a three phase self-excited induction generator*, IEEE Transaction on Industrial Application, vol. 40, no. 4, pp. 978–988 (2004).

[17] Subramaniam S.K., Natarajan K., Muthiah S., Mahendhar R., *Modelling, analysis and control of stand-alone self-excited induction generator-pulse width modulation rectifier systems feeding constant DC voltage applications*, IET Generation Transmission and Distribution., vol. 8, no. 6, pp. 1140–1155 (2014).

[18] Murthy S.S., Singh B.P., Nagamani C., Satyanarayana K.V.V., *Studies on the use of conventional induction motors as self-excited induction generators*, IEEE Transaction on Energy Conversion, vol. 3, no. 4, pp. 842–848 (1988).

[19] Bodson M., Kiselychnyk O., *Analysis of Triggered Self-Excitation in Induction Generator and Experimental Validation*, IEEE Transaction on Energy Conversion, vol. 27, no. 2, pp. 238–249 (2012).

[20] Kalamen L., Rafajdus P., Sekerak P., Hrabovcova V., *A novel method of magnetizing inductance investigation of self-excited induction generators*, IEEE Transactions on Magnetics, vol. 48, no. 4, pp. 1657–1660 (2012).

[21] Harrington R.J., Bassiouny F.M.M., *New approach to determine the critical capacitance for self-excited induction generators*, IEEE Transaction on Energy Conversion, vol. 13, no. 3, pp. 244–249 (1998).

[22] Kheldoun A., Refoufi L., Khodja D.E., *Analysis of the self-excited induction generator steady state performance using a new efficient algorithm*, Electric Power System Research, 86, pp. 61–67 (2012).

[23] Brudny J.F., Pusca R., Roisse H., *Wind turbines using self-excited three-phase induction generators: an innovative solution for voltage-frequency control*, European Physical Journal Applied Physics, vol. 43, pp. 173–187 (2008).

[24] Gordon R.S., *Modelling of induction machines for electric drives*, IEEE Transaction on Industrial Application, vol. 25, no. 6, pp. 1126–1131 (1989).

[25] Levi E., *A unified approach to main flux saturation modelling in D-Q axis models of induction machines*, IEEE Transaction on Energy Conversion, vol. 10, no. 3, pp. 455–461 (1995).

[26] Moulahoum S., Baghli L., Rezzoug A., Touhami O., *Sensorless Vector Control of a Saturated Induction Machine accounting for iron loss*, European Journal of Electrical Engineering, Lavoisier, Hermès Sciences, vol. 11, no. 4/5, pp. 511–543 (2008).

[27] Idjdarene K., Rekioua D., Rekioua T., *Performance of an isolated induction generator under unbalanced loads*, IEEE Transaction on Energy Conversion, vol. 25, no. 2, pp. 303–311 (2010).

[28] Hallenius K.E., Vas P., Brown J., *The analysis of a saturated self-excited asynchronous generator*, IEEE Transaction on Energy Conversion, vol. 6, no. 2, pp. 336–345 (1991).

[29] Touti E., Pusca R., Manata J.P., Brudny J.F., Châari A., *On the use of a dimmer for a robust frequency control of a self-excited three-phase induction wind generator*, Journal of Power Electronics, vol. 12, no. 4, pp. 1–12 (2014).

[30] Ababsa M.L., Ninet O., Velu G., Lecointe J.P., *High-Temperature Magnetic Characterization Using an Adapted Epstein Frame*, IEEE Transactions on Magnetics, vol. 54, iss. 6 (2018).